

The anatomy, organisation and development of contralateral callosal projections of the mouse somatosensory cortex

Brain and Neuroscience Advances

Volume 1: 1–9

© The Author(s) 2017

Reprints and permissions:

sagepub.co.uk/journalsPermissions.nav

DOI: 10.1177/2398212817694888

journals.sagepub.com/home/bnaLaura R. Fenlon¹, Rodrigo Suárez¹ and Linda J. Richards^{1,2}

Abstract

Background: Alterations in the development of neuronal connectivity can result in dramatic outcomes for brain function. In the cerebral cortex, most sensorimotor and higher-order functions require coordination between precise regions of both hemispheres through the axons that form the corpus callosum. However, little is known about how callosal axons locate and innervate their contralateral targets.

Methods: Here, we use a combination of in utero electroporation, retrograde tracing, sensory deprivation and high-resolution axonal quantification to investigate the development, organisation and activity dependence of callosal axons arising from the primary somatosensory cortex of mice.

Results: We show that distinct contralateral projections arise from different neuronal populations and form homotopic and heterotopic circuits. Callosal axons innervate the contralateral hemisphere following a dorsomedial to ventrolateral and region-specific order. Furthermore, we identify two periods of region- and layer-specific developmental exuberance that correspond to initial callosal axon innervation and subsequent arborisation. Early sensory deprivation affects only the latter of these events.

Conclusion: Taken together, these results reveal the main developmental events of contralateral callosal targeting and may aid future understanding of the formation and pathologies of brain connectivity.

Keywords

Corpus callosum, cortical development, contralateral targeting, activity dependence

Received: 21 December 2016; accepted: 30 January 2017

Introduction

The corpus callosum is the largest fibre tract in the human brain. It comprises axons that mediate the integration of sensory, motor and associative functions between the cerebral hemispheres (Aboitiz and Montiel, 2003; Edwards et al., 2014; Gobius and Richards, 2011; Paul et al., 2007). These interhemispheric circuits are mostly homotopic; that is, they project to regions similar to those from which they arise (Yorke and Caviness, 1975), and the spatial distribution of contralateral axons correlates with the dorsoventral position of axons along the callosal tract (Zhou et al., 2013). However, callosal circuits also include heterotopic projections, such as those described between different cortical regions or from primary cortices to the contralateral striatum (Boyd et al., 1971; Sohur et al., 2014; Suárez et al., 2014; Veinante and Deschênes, 2003; Wilson, 1987). Moreover, as not all cortical regions project or receive axons contralaterally in the adult (Innocenti et al., 1977; Ivy et al., 1979; Ivy and Killackey, 1981; Olavarria and van Sluyters, 1985; O'Leary et al., 1981), the specification of contralateral circuits is likely to involve multiple developmental mechanisms. Interestingly, homotopic and heterotopic callosal circuits are differentially affected by manipulations of sensory and spontaneous activity during critical periods of postnatal development (Huang et al., 2013; Mizuno et al., 2007, 2010; Suárez et al., 2014; Wang et al., 2007), further implying the existence of region- and context-specific targeting mechanisms.

The formation and stabilisation of callosal projections, including axonal targeting, exuberance and retraction have, been only partially described, and conflicting hypotheses have been proposed, likely reflecting different experimental approaches (see Fenlon and Richards, 2015 for review). For example, three scenarios have been suggested to explain how transient callosal axons initially target the contralateral hemisphere before retracting: (1) they project exclusively to areas that receive callosal projections in the adult (Olavarria and van Sluyters, 1985), (2) they remain in deep layers of prospective regions that will become both callosally and non-callosally innervated in the adult (Innocenti, 1981) or (3) they innervate the entire cortical plate of prospective callosal and non-callosal regions (Elberger, 1994). Here, we employed a highly replicable labelling technique, involving in utero electroporation

¹Queensland Brain Institute, The University of Queensland, Brisbane, QLD, Australia

²School of Biomedical Sciences, The University of Queensland, Brisbane, QLD, Australia

Corresponding author:

Linda J. Richards, Queensland Brain Institute, The University of Queensland, Brisbane, QLD 4072, Australia.

Email: richards@uq.edu.au



of fluorescent proteins and high-resolution axonal quantifications, to investigate these possibilities in a model that contains both homotopic and heterotopic callosal projections: the mouse somatosensory system. The advantages of this method are that it can be targeted to label specific populations of neurons in the cortex, it provides whole cell fills and it avoids the presence of a fluorescent bolus at the injection site (Kozulin et al., 2016). By analysing contralateral axon development at multiple time points and under paradigms of sensory manipulation, we present a scheme that incorporates elements from previously conflicting hypotheses, which could serve as a new experimental model to study bilateral brain wiring under healthy and pathological conditions.

Materials and methods

In utero electroporation, cauterisation and tissue collection

All animal procedures were approved by The University of Queensland Animal Ethics Committee. To perform *in utero* electroporation, pregnant CD1 mouse dams underwent laparotomy at embryonic day (E) 15.5, and the lateral ventricle of embryos was injected with 0.5–1 μ L of pCAG-eYFP (yellow fluorescent protein; from Tetsuichiro Saito, Chiba University, Chiba, Japan; 1 μ g/ μ L) in the case of animals that were subsequently studied at postnatal days (P) 4–20, or pCAG-piggybac-GFP (green fluorescent protein) and pCAG-piggybac-transposase (0.75 μ g/ μ L each; both from Joseph LoTurco, University of Connecticut, Mansfield, CT, USA) in the case of animals studied at P50. The presumptive primary somatosensory cortex (S1) was then electroporated with five 100 ms pulses at 36 V using 3-mm paddle electrodes. For the cauterisation experiments, the whisker pad opposite to the electroporated hemisphere was lightly cauterised at the follicular surface of P3 pups under ice anaesthesia. Animals (of mixed sex) were collected at different developmental ages (P4, P5, P6, P7, P8, P10, P12, P15, P20 and P50), anaesthetised with sodium pentobarbital and perfused transcardially with 0.9% NaCl followed by 4% paraformaldehyde. For developmental analyses, different time points were studied within single litters where possible to reduce the impact of any potential inter-litter variability on experimental conditions. Live pups were examined for intensity, size and position of fluorescence in the somatosensory cortex using a dissection microscope equipped with epifluorescence at P1–2, and only those with appropriate labelling were selected for further processing. Flat-mount cortical samples were prepared by compressing freshly perfused cortices and immersing them in paraformaldehyde for 2 days pressed between two glass slides, as described previously (Fenlon et al., 2015).

Immunohistochemistry

The primary antibodies used were chicken anti-GFP (1:750; Abcam, Cambridge, UK) alone or with rabbit anti-VGLUT2 (vesicular glutamate transporter 2; 1:750; Synaptic Systems, Göttingen, Germany) to clearly demarcate the barrel field in S1, followed by goat anti-chicken 488 and goat anti-rabbit 555 Alexa Fluor IgG secondary antibodies, respectively (1:500; Invitrogen, Carlsbad, CA, USA) and 4',6-diamidino-2-phenylindole, dihydrochloride (DAPI) staining on 50- μ m coronal sections. Only those animals with electroporated cell bodies in layer (L)2/3 of the entire S1 were selected for further analyses.

Stereotaxic injection of retrograde tracer

Adult male and female CD1 mice (>P30) were anaesthetised with isoflurane (1%–4% in oxygen at 200 mL/kg/min) in a mouse stereotaxic unit. The skull was exposed and holes were drilled above coordinates (relative to bregma) corresponding to the right primary somatosensory/secondary somatosensory cortex (S1/S2) border (anterior–posterior = -1.34 , medial–lateral = 3.5 , dorsal–ventral = -1.9) and the insular/perirhinal area (Ins/PRh) (anterior–posterior = -1.34 , medial–lateral = 4.35 , dorsal–ventral = -3.65) (Paxinos et al., 2007). A pulled glass pipette was then used to iontophoretically inject the carbocyanines DiI or DiD (10 mg/mL dissolved in dimethyl sulfoxide) into each site at 1 μ A, 7 s on/off alternation, for 10 min at each site. The incision was then sutured, and the mice were sacrificed after 8 days.

Fluorescence intensity analysis

The fluorescence intensity during the developmental time course was analysed using a custom MATLAB program. Sections within the posterior medial barrel subfield, which represent inputs from the mystacial whiskers, were chosen for analyses. Brain sections were examined for the density and position of fluorescently labelled cell bodies, as well as the brightness and laminar distribution of the cell field. The labelling of cells within L2/3 of the cortex was consistent and specific across experiments, with only one or two L5 cells labelled in each brain section and no instances of alternative laminar position of the cell field. Brains with inappropriate labelling in any of these criteria were excluded from further analysis. Sections containing S1 and S2 were selected using anatomical landmarks identified with DAPI staining and reference to a developmental mouse brain atlas (Paxinos et al., 2007), as well as VGLUT2 staining to precisely outline the barrel field (Suárez et al., 2014). The width of each cortical layer and of the entire cortical plate (revealed by DAPI staining) was determined to design appropriately scaled and comparable regions of interest specific for each age group. The average fluorescence intensity was determined across 200 evenly spaced horizontal bins across the entire cortical plate. A sample of background auto-fluorescence in the hippocampus within each section was measured and used for normalisation. The normalised fluorescence value of axons is labelled as $f/f_{\text{bg tissue}}$ in Figures 3–5: axonal fluorescence/fluorescence of background tissue containing no label. For layer-specific analyses, values comprising 10% of the width of each layer were obtained from the centre of each layer. Normality of distribution for all data sets to be statistically compared (all $n \geq 7$ animals per condition) was confirmed with Shapiro–Wilk tests, and unpaired two-tailed Student's *t* tests were performed to compare individual ages within a single area and/or layer.

Results

Callosal axons project to discrete homotopic and heterotopic areas of the contralateral cortex in the juvenile and adult mouse

To consistently label callosal axons from S1, we performed *in utero* electroporation of eYFP in the presumptive S1 of E15.5 mice and analysed animals with consistent labelling of L2/3 callosal neurons. In order to investigate the spatial distribution and

developmental stability of these projections, we compared coronal brain sections collected at P10 and P50 and found that dense callosal projections to S1/S2 and Ins/PRh, as well as the sparse projections to S1 and S2, are present at P10 (Figure 1(a)) and are maintained into adulthood (Figure 1(b)). Next, we examined electroporated P10 brains in tangential flat mounts (Figure 1(c) and (d)) to characterise the spatial distribution of these projections with respect to each cortical area. We found that whereas the S1/S2 projection innervates the entire latero-caudal edge of the principal whisker barrel subfield (Figure 1(d)), the Ins/PRh projection is confined to a smaller region at the borders between the posterior insular cortex and anterior perirhinal cortex both ipsilaterally and contralaterally (Figure 1(c) and (d)).

Homotopic and heterotopic callosal projections from S1 arise from distinct neuronal populations

Given that this was one of the first reported instances of a homotopic and heterotopic callosal projection arising from a single cortical area, it was important to determine whether these dense callosal projections originate from independent cell populations or whether single neurons branch to both targets. We performed double in vivo stereotaxic injections of DiI and DiD in S1/S2 and Ins/PRh and examined the spatial position and degree of colocalisation of retrogradely labelled cell bodies in the contralateral hemisphere 8 days later (Figure 2(a)). Retrograde labelling from these two injection sites revealed fasciculated axon bundles in the callosal tract, with the S1/S2 axons located more dorsally and the Ins/PRh axons more ventrally (Figure 2(a')). Moreover, whereas most of the retrogradely labelled cell bodies are located in regions homotopic to the injection sites (Figure 2(a) and (b)), some cells in each region also labelled with the dye corresponding to the heterotopic region (Figure 2(a'') and (a'''); arrowheads). However, regardless of the injection site or region of interest for cell-body quantifications, virtually no cells incorporated both dyes, suggesting that although neurons with homotopic and heterotopic projection phenotypes can be found across S1, the distinct contralateral projections observed from in utero electroporation arise from independent neuronal populations (Figure 2(a) and (c)).

Callosal projections enter the contralateral cortex in a dorsomedial to ventrolateral and region-specific manner

An important aspect of callosal connectivity is that axons form dense region- and layer-specific arbours in the contralateral hemisphere. However, how callosal axons develop this specific pattern of connectivity in mice is currently unknown. We investigated the developmental sequence that callosal projections undergo when innervating the contralateral hemisphere by quantifying the relative number of YFP-positive callosal axons across cortical layers in the contralateral target regions (S1, S1/S2, S2 and Ins/PRh) over nine stages of postnatal development (P4, P5, P6, P7, P8, P10, P12, P15 and P20). Callosal axons reach the white matter of the contralateral cortex by P4 (Figure 3(a)), as previously shown (Wang et al., 2007). By P5, callosal axons start to innervate the deep layers of S1 (yellow trace, Figure 3(b)), followed

by the S1/S2 and S2 regions at P6 (red and purple traces, Figure 3(c)). This suggests that axonal innervation of the cortical plate follows a continuous dorsomedial to ventrolateral progression, following the growth of the callosal tract. Interestingly, less densely innervated callosal regions (e.g. S2; Figure 2 purple traces) do not display periods of comparatively high axonal innervation, suggesting the involvement of a mechanism that regulates the initial region-specific targeting of these axons. This conclusion is strengthened by our frequent observation of early innervating axons that extend specifically into the cortical plate at the S1/S2 border, but not in surrounding regions (Figure 3(b'), arrowhead). Within the S1/S2 region, however, axons initially populate the cortical plate without layer-specific arborisation patterns (P7; Figure 3(d) and (d')), before starting to arborise in all layers except L4 from P8 (Figure 3(e)–(i), red traces). In contrast to the earlier (P8) distinction of the S1/S2 projection, the Ins/PRh has a fluorescence intensity profile that is distinguishable from the other projections (S1 and S2) at the later stage of P10 (Figure 3; green traces), a delay that could be explained by the dorsomedial to ventrolateral sequence of innervation.

Spatially and temporally specific events of exuberance and elimination of callosal axons

Whether and how corpus callosum formation involves developmental exuberance and elimination of axons are currently unclear. For example, whether axonal exuberance and elimination is a homogeneous or region-specific process, and the transient fate of exuberant axons prior to elimination, remain unresolved questions (reviewed in Fenlon and Richards, 2015). To address this, we examined the temporal progression of callosal innervation across cortical layers and regions (Figure 4(a)–(d)). We found that the innervation of deep and upper layers progresses in spatially and temporally distinct ways. In deep layers, we observed a significant peak of axonal fluorescence by P7 across all regions studied (S1, S1/S2, S2 and Ins/PRh), which by P20 drops to similar levels to those displayed during initial axon innervation in S1, S1/S2 and S2 (Figure 4(e)–(h), Table 1). In contrast, axonal fluorescence in upper layers progressively increases until P10 across all cortical regions. We also found spatial differences in the extent of axonal elimination. In the sparsely innervated S1 and S2, axonal presence in upper layers increases in a steady manner between P4 and P20 (Figure 4(e) and (g), Table 1), and there is no evidence of axonal retraction. However, in the more densely innervated projections to the S1/S2 border and to the Ins/PRh region, axonal presence in the upper layers peaks at P10 and then shows a significant decline, although to a lesser extent than the pattern exhibited in deep layers (Figure 4(j) and (l), Table 1). Taken together, these data identify two temporal and spatial events of axonal exuberance and elimination in the contralateral hemisphere: one that peaks at P7 in deep layers for all cortical areas studied and another that peaks at P10 in the upper layers of the most densely innervated areas.

Sensory deprivation affects the second but not the first peak of axonal exuberance

Given that exuberance and elimination of callosal axons differ between layers and regions, and that disrupting activity during

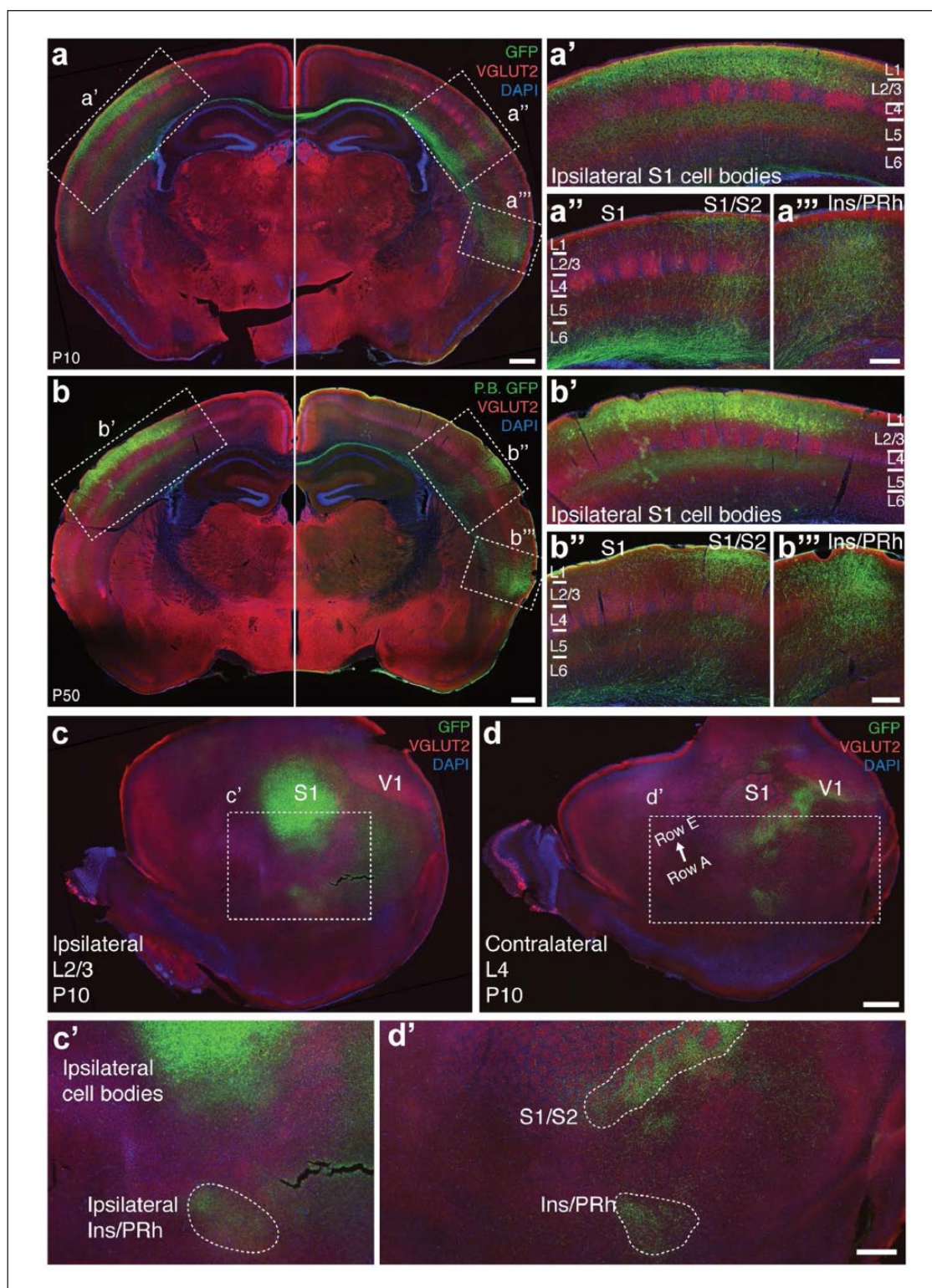


Figure 1. A characterisation of the callosal projections that result from L2/3 S1 in utero electroporation at E15.5. (a) Labelling these cells and examining the brain in the coronal plane at P10 reveals (a') diffuse labelling of S1, (a'') a dense projection into the S1/S2 border region, (a''') diffuse labelling in S2 and a dense projection into the Ins/PRh cortex. (b)–(b''') This pattern is maintained into adulthood (P50). Tangential sections through the (c) electroporated and (d) contralateral hemispheres of a P10 brain confirm a projection to the (c') ipsilateral Ins/Prh region and that the S1/S2 projection extends along a longer anterior–posterior axis than the Ins/PRh projection in the (d') contralateral hemisphere. $n = 3$ animals for each condition. Scale bars: 500 μm for (a) and (b) and (c') and (d'), 250 μm for (a) and (b) insets, 1000 μm for (c) and (d).

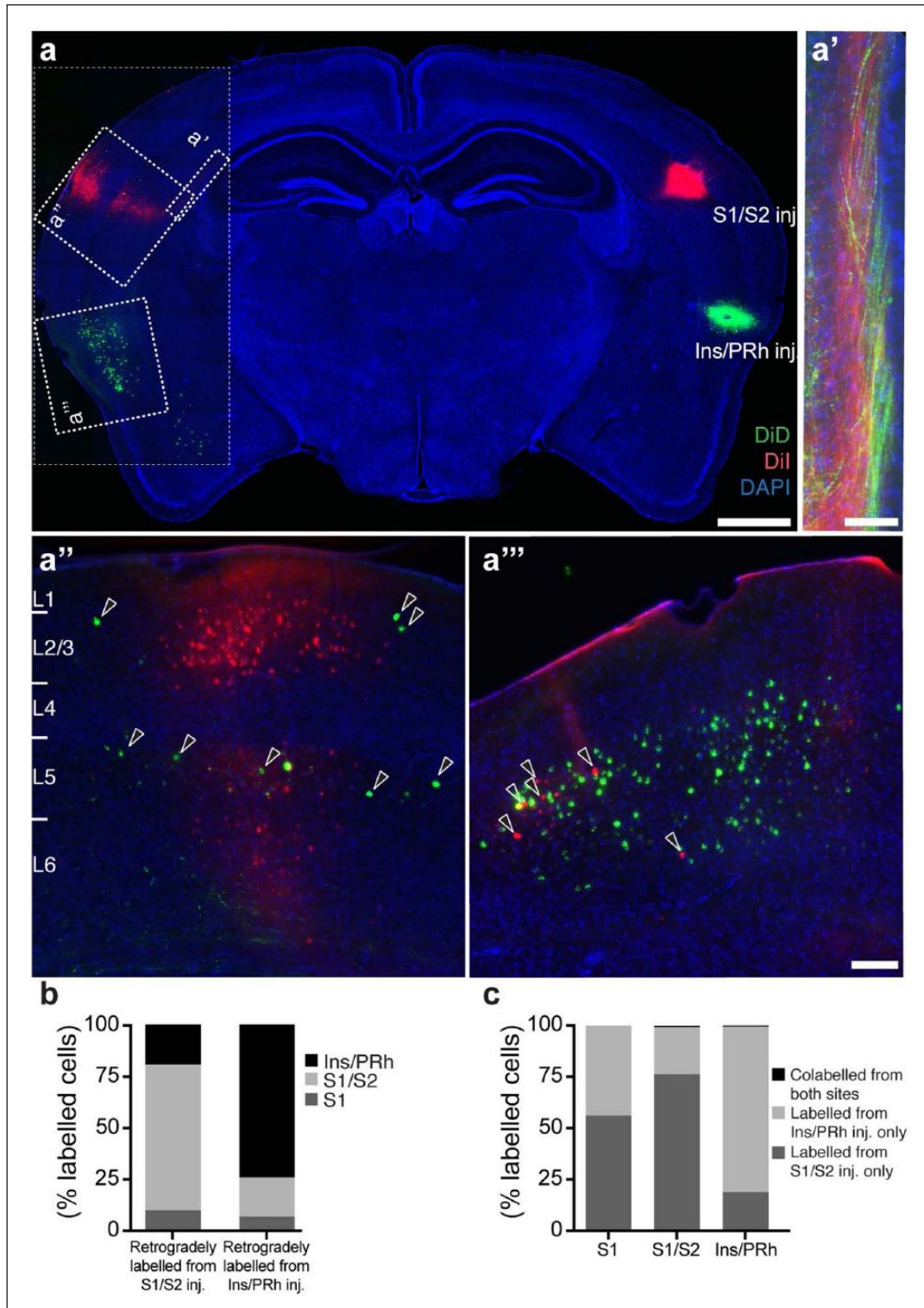


Figure 2. Cellular origins of S1/S2 and Ins/PRh callosal projections. Retrograde tracing experiments reveal the organisation of the S1/S2 and Ins/PRh projections. (a) DiI/DiD (red/green) injections into the S1/S2 and Ins/PRh cortex showed a generally homotopic pattern of contralaterally labelled cell bodies and (a') a segregated arrangement within the white matter, where axons projecting to S1/S2 are located more dorsomedially than axons projecting to Ins/PRh. There are, however, some retrogradely labelled cell bodies in the heterotopic location and these predominantly do not colocalise with homotopically labelled cells (a'' and a'''; arrowheads). These results are also reflected upon quantification of labelled cell number (b) in different areas and (c) degree of colocalisation. $n = 3$ animals for each condition. Scale bars: 1000 μm for (a), 500 μm for (a'), 100 μm for (a'') and (a''').

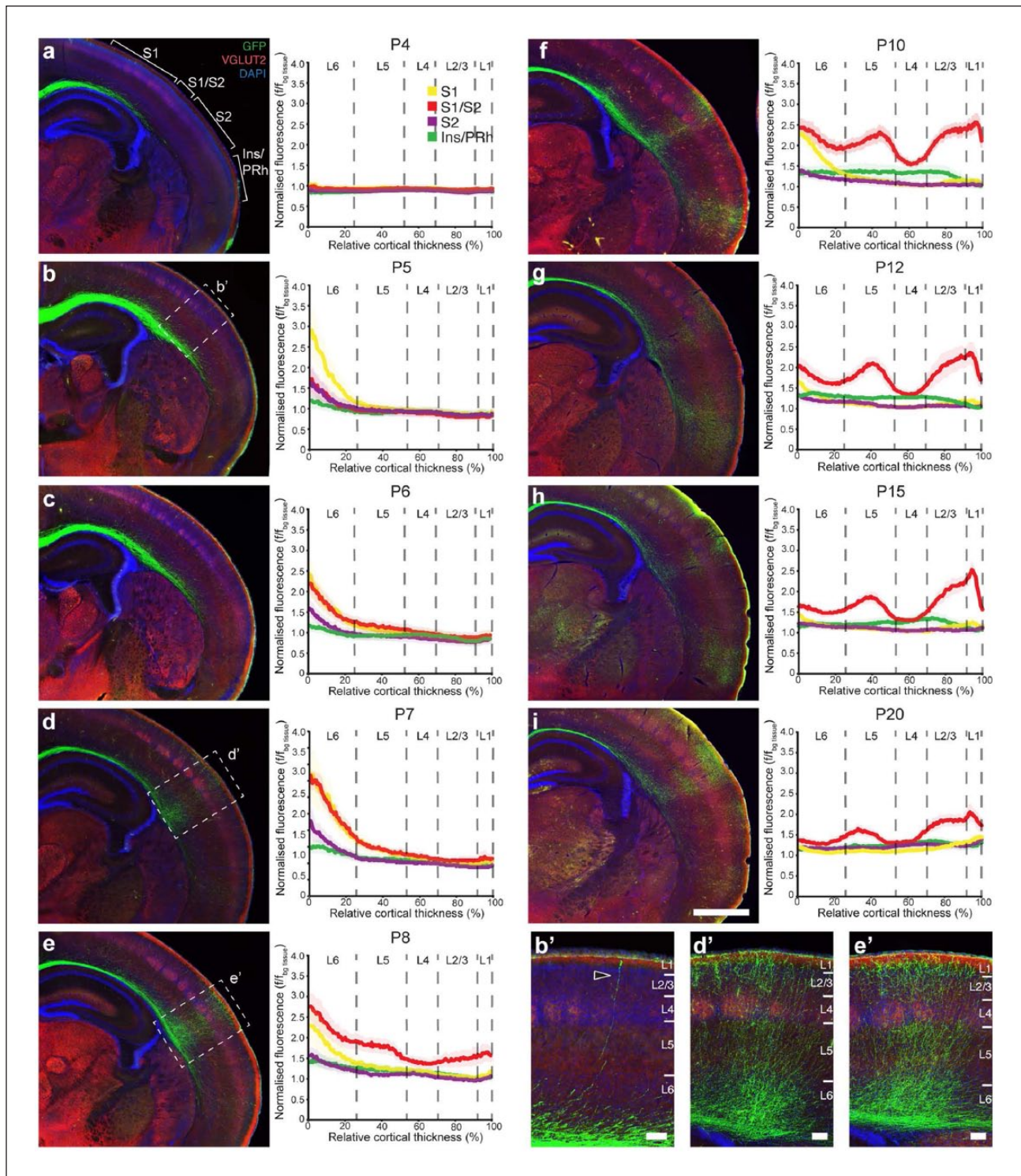


Figure 3. The development of contralateral axonal innervation of L2/3 S1 callosal neurons. Photomicrographs and densitometric line scans of axonal fluorescence intensity through S1 (yellow), S1/S2 (red), S2 (purple) and Ins/PRh (green) of mouse brains electroporated into L2/3 of S1 at E15.5 and collected at (a) P4 and (b and b') P5. A detailed examination of the process of contralateral callosal targeting throughout development was obtained by examining stages (c) P6, (d and d') P7, (e and e') P8, (f) P10, (g) P12, (h) P15 and (i) P20. The graphs represent the entire cortical thickness of each layer, divided into six cortical layers that apply to S1, S1/S2 and S2 but not Ins/PRh, which is not a six-layered structure. $f/f_{bg \text{ tissue}}$: axonal fluorescence/fluorescence of background tissue. Data are represented as mean \pm SEM. $n \geq 7$ animals per age. Scale bars: 1000 μm for (a)–(i) and 100 μm for insets.

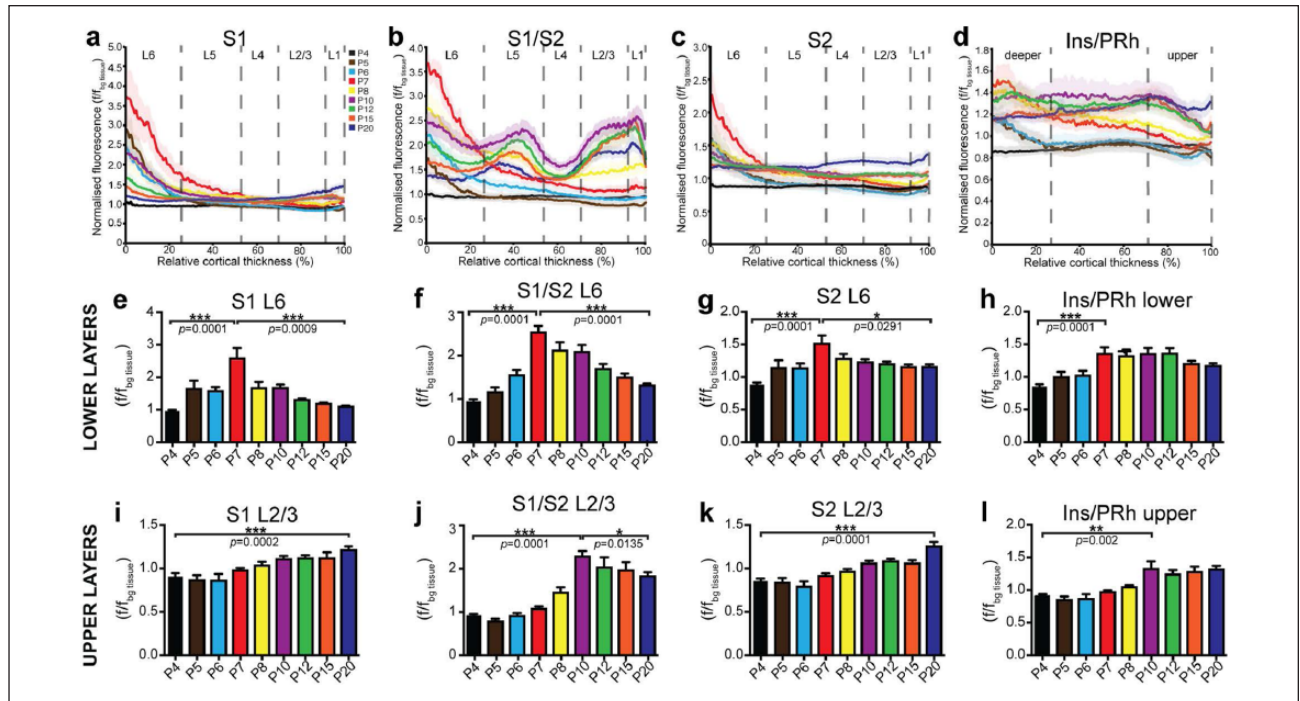


Figure 4. Two periods of temporally, regionally, and layer-specific developmental exuberance in L2/3 S1 callosal neuron projections. Densitometric fluorescence analyses of labelled axons were assessed over nine developmental stages to obtain average traces for each age across the cortical plate in (a) S1, (b) S1/S2, (c) S2 and (d) Ins/PRh across different stages of development. (e)–(h) The average fluorescence intensity of each layer reveals a distinct peak of fluorescence at P7 (red) in L6 of all neocortical areas and possibly lower layers of Ins/PRh. The future sparsely innervated regions (S1 and S2) generally have a linear increase in fluorescence intensity in (i) and (k) upper cortical layers, whereas the densely innervated regions trend towards a peak of fluorescence at P10, followed by (j) and (l) slight retraction. $f/f_{bg\ tissue}$: axonal fluorescence/fluorescence of background tissue. Data are represented as mean \pm SEM. $n \geq 7$ animals per age.

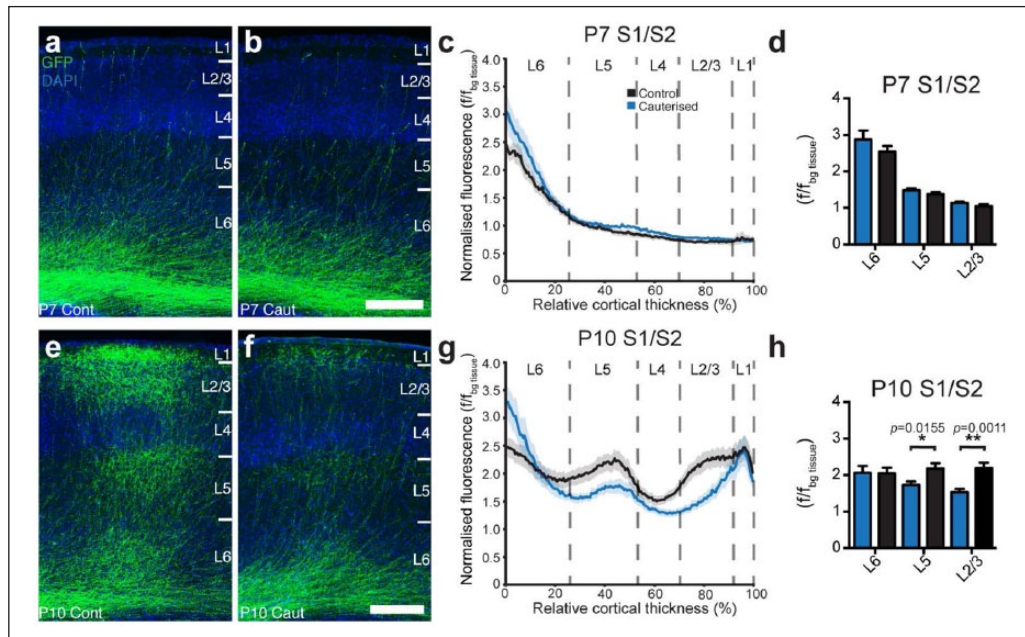


Figure 5. Unilateral sensory deprivation inhibits developmental exuberance of axonal arbours but not initial axon targeting. (a)–(d) Unilateral cauterisation at P3 results in no change in axonal innervation in any cortical layer of S1/S2 by P7. (e)–(h) However, the same manipulation causes a significant change in axonal presence in L2/3 and 5 (but not L6) when examined at P10. $f/f_{bg\ tissue}$: axonal fluorescence/fluorescence of background tissue. Data are represented as mean \pm SEM. $n \geq 7$ animals per condition. Scale bars: 250 μ m.

Table 1. Statistics.

Figure	Data compared	Data structure	Type of test	<i>p</i> value
4(e)	Lower layers S1 P4 versus P7	Normal distribution	Two-way unpaired Student's <i>t</i> test	0.0001
4(e)	Lower layers S1 P7 versus P20	Normal distribution	Two-way unpaired Student's <i>t</i> test	0.0009
4(f)	Lower layers S1/S2 P4 versus P7	Normal distribution	Two-way unpaired Student's <i>t</i> test	0.0001
4(f)	Lower layers S1/S2 P7 versus P20	Normal distribution	Two-way unpaired Student's <i>t</i> test	0.0001
4(g)	Lower layers S2 P4 versus P7	Normal distribution	Two-way unpaired Student's <i>t</i> test	0.0001
4(g)	Lower layers S2 P7 versus P20	Normal distribution	Two-way unpaired Student's <i>t</i> test	0.0291
4(h)	Lower layers Ins/PRh P4 versus P7	Normal distribution	Two-way unpaired Student's <i>t</i> test	0.0001
4(h)	Lower layers Ins/PRh P7 versus P20	Normal distribution	Two-way unpaired Student's <i>t</i> test	0.1234
4(i)	Upper layers S1 P4 versus P20	Normal distribution	Two-way unpaired Student's <i>t</i> test	0.0002
4(j)	Upper layers S1/S2 P4 versus P10	Normal distribution	Two-way unpaired Student's <i>t</i> test	0.0001
4(j)	Upper layers S1/S2 P10 versus P20	Normal distribution	Two-way unpaired Student's <i>t</i> test	0.0135
4(k)	Upper layers S2 P4 versus P20	Normal distribution	Two-way unpaired Student's <i>t</i> test	0.0001
4(l)	Upper layers Ins/PRh P4 versus P10	Normal distribution	Two-way unpaired Student's <i>t</i> test	0.002
4(l)	Upper layers Ins/PRh P10 versus P20	Normal distribution	Two-way unpaired Student's <i>t</i> test	0.9475
5(d)	P7 S1/S2 L6 cont. versus caut.	Normal distribution	Two-way unpaired Student's <i>t</i> test	0.3157
5(d)	P7 S1/S2 L5 cont. versus caut.	Normal distribution	Two-way unpaired Student's <i>t</i> test	0.1652
5(d)	P7 S1/S2 L2/3 cont. versus caut.	Normal distribution	Two-way unpaired Student's <i>t</i> test	0.1072
5(h)	P10 S1/S2 L6 cont. versus caut.	Normal distribution	Two-way unpaired Student's <i>t</i> test	0.9599
5(h)	P10 S1/S2 L5 cont. versus caut.	Normal distribution	Two-way unpaired Student's <i>t</i> test	0.0155
5(h)	P10 S1/S2 L2/3 cont. versus caut.	Normal distribution	Two-way unpaired Student's <i>t</i> test	0.0011

Caut.: cauterised; cont.: control; Ins/PRh: insular/perirhinal area; S1: primary somatosensory cortex; S2: secondary somatosensory cortex; S1/S2 border between S1 and S2 cortices.

a critical period affects callosal projections in a layer- and region-specific manner (Suárez et al., 2014), we next studied whether and how sensory deprivation affects axonal exuberance and elimination. We performed unilateral cauterisations of one whisker pad on mouse pups at P3 (during the critical period of callosal development) and examined axon fluorescence at P7 and P10 during the two peaks of axonal exuberance. We found that sensory deprivation did not affect axonal innervation to any layer at P7 (Figure 5(a)–(d), Table 1), but decreased axonal presence in the arborised layers (L2/3 and L5) at P10 (Figure 5(e)–(h), Table 1). These results suggest that whereas the initial innervation of callosal axons is activity-independent, later arborisation and stabilisation of region-specific callosal connections require activity-dependent mechanisms.

Discussion

The coexistence of heterotopic and homotopic projections arising from distinct neurons located within the same cortical regions and layers suggests that specification of callosal targets involves additional mechanisms to spatial cues alone. For example, region-specific callosal projections are differentially affected by balanced activity across hemispheres (Huang et al., 2013; Suárez et al., 2014). Our findings of a dorsomedial to ventrolateral pattern of contralateral axon innervation are in accordance with previous findings, whereby contralateral innervation recapitulates the dorsoventral axonal arrangement within the callosal tract (Zhou et al., 2013). However, we also reveal a combination of spatial and temporal events, from initial innervation and arborisation to exuberance and elimination of contralateral terminals, that likely reflects interactions of several developmental mechanisms.

The first peak of callosal axon exuberance at P7 likely represents axons sampling their environment, mostly within the deeper

layers; these axons would subsequently either retract or further innervate the overlying cortex, as previously hypothesised in cats (Aggoun-Zouaoui and Innocenti, 1994; Innocenti, 1981; Innocenti and Clarke, 1984). In contrast, the second exuberance event at P10 likely represents an overproduction of axonal branches that later disappear, as previously described in cats (Aggoun-Zouaoui et al., 1996; Bressoud and Innocenti, 1999). It is unclear from the available data whether this retraction of branches involves whole axonal retraction or localised pruning of axonal arbours; however, the presence of a similar retraction trend within the less-arborised L4 of the S1/S2 projection (Figure 4(b)) suggests at least some degree of axonal elimination. This study has enabled two temporally and spatially distinct events of callosal exuberance to be investigated within the same model system. Thus, the first and second hypotheses of contralateral positioning of excess callosal axons, which state that (1) they project exclusively to areas that receive callosal projections in the adult or (2) they remain in deep layers of prospective regions that will become both callosally and non-callosally innervated in the adult, are both supported by this study in a rodent model. However, we did not find any evidence for the third hypothesis; that is, that excess callosal axons innervate the entire cortical plate of prospective callosal and non-callosal regions and then retract to produce the adult innervation pattern. Our results have therefore identified crucial stages of axonal targeting and arborisation in the rodent and provide a more unified paradigm of contralateral callosal targeting.

Spontaneous and sensory-evoked neuronal activities have been previously shown to differentially affect axonal targeting to different cortical regions (Huang et al., 2013; Suárez et al., 2014). Here, we extend these findings and suggest that although initial axon exploration in deep layers might be independent of activity, region- and layer-specific arborisation and the stabilisation of callosal terminals involve activity-dependent mechanisms. This

model is consistent with previous evidence showing that sensory manipulations until P7 can disrupt callosal targeting in mice (Huang et al., 2013).

In conclusion, our results reveal previously uncharacterised anatomical features of callosal development that incorporate proposed mechanisms from previously conflicting studies. By carefully examining the formation of bilateral circuits in a spatially and temporally specific manner using high-resolution fluorescence imaging, this study also presents novel experimental assays that could be used for mechanistic studies of each of these processes in healthy conditions, as well as in mouse models of human neurodevelopmental diseases.

Acknowledgements

The authors thank J Bertran-Gonzalez for training on and use of the stereotaxic injection equipment, as well as I Gobius and R Tweedale for comments on the manuscript and The University of Queensland Biological Resources and Queensland Brain Institute for animal support. L.R.F., R.S. and L.J.R. designed experiments and wrote the paper. L.R.F. performed the experiments, analysed the data and prepared the figures.

Declaration of conflicting interests

The author(s) declared no potential conflicts of interest with respect to the research, authorship and/or publication of this article.

Funding

This work was funded by National Health and Medical Research Council (NHMRC) project grants 1029975 and 1064174. L.R.F. was supported by an Australia Postgraduate Award, R.S. by an Australian Research Council (ARC) Discovery Early Career Researcher Award 160101394 and L.J.R. by a NHMRC Principal Research Fellowship 1005751. The content is solely the responsibility of the authors and does not necessarily represent the official views of the NHMRC or the ARC.

References

Aboitiz F and Montiel J (2003) One hundred million years of interhemispheric communication: The history of the corpus callosum. *Brazilian Journal of Medical and Biological Research* 36(4): 409–420.

Aggoun-Zouaoui D and Innocenti GM (1994) Juvenile visual callosal axons in kittens display origin- and fate-related morphology and distribution of arbors. *European Journal of Neuroscience* 6(12): 1846–1863.

Aggoun-Zouaoui D, Kiper DC and Innocenti GM (1996) Growth of callosal terminal arbors in primary visual areas of the cat. *European Journal of Neuroscience* 8(6): 1132–1148.

Boyd EH, Pandya DN and Bignall KE (1971) Homotopic and nonhomotopic interhemispheric cortical projections in the squirrel monkey. *Experimental Neurology* 32(2): 256–274.

Bressoud R and Innocenti GM (1999) Typology, early differentiation, and exuberant growth of a set of cortical axons. *Journal of Comparative Neurology* 406(1): 87–108.

Edwards TJ, Sherr EH, Barkovich AJ, et al. (2014) Clinical, genetic and imaging findings identify new causes for corpus callosum development syndromes. *Brain* 137(6): 1579–1613.

Elberger AJ (1994) Transitory corpus callosum axons projecting throughout developing rat visual cortex revealed by Dil. *Cerebral Cortex* 4(3): 279–299.

Fenlon LR and Richards LJ (2015) Contralateral targeting of the corpus callosum in normal and pathological brain function. *Trends in Neurosciences* 38(5): 264–272.

Fenlon LR, Liu S, Gobius I, et al. (2015) Formation of functional areas in the cerebral cortex is disrupted in a mouse model of autism spectrum disorder. *Neural Development* 10(1): 10.

Gobius I and Richards L (2011) *Creating Connections in the Developing Brain: Mechanisms Regulating Corpus Callosum Development* (2nd edn, Colloquium Series on the Developing Brain). Williston, VT: Morgan & Claypool Publishers, pp. 1–48.

Huang Y, Song N-N, Lan W, et al. (2013) Sensory input is required for callosal axon targeting in the somatosensory cortex. *Molecular Brain* 6(1): 53.

Innocenti GM (1981) Growth and reshaping of axons in the establishment of visual callosal connections. *Science* 212(4496): 824–827.

Innocenti GM and Clarke S (1984) The organization of immature callosal connections. *Journal of Comparative Neurology* 230(2): 287–309.

Innocenti GM, Fiore L and Caminiti R (1977) Exuberant projection into the corpus callosum from the visual cortex of newborn cats. *Neuroscience Letters* 4(5): 237–242.

Ivy GO, Akers RM and Killackey HP (1979) Differential distribution of callosal projection neurons in the neonatal and adult rat. *Brain Research* 173(3): 532–537.

Ivy GO and Killackey HP (1981) The ontogeny of the distribution of callosal projection neurons in the rat parietal cortex. *Journal of Comparative Neurology* 195(3): 367–389.

Kozulin P, Almaraz G, Gobius I, et al. (2016) Investigating early formation of the cerebral cortex by in utero electroporation: Methods and protocols. In: Walker DW (ed.) *Prenatal and Postnatal Determinants of Development*. New York: Springer, pp. 3–20.

Mizuno H, Hirano T and Tagawa Y (2007) Evidence for activity-dependent cortical wiring: Formation of interhemispheric connections in neonatal mouse visual cortex requires projection neuron activity. *Journal of Neuroscience* 27(25): 6760–6770.

Mizuno H, Hirano T and Tagawa Y (2010) Pre-synaptic and post-synaptic neuronal activity supports the axon development of callosal projection neurons during different post-natal periods in the mouse cerebral cortex. *European Journal of Neuroscience* 31(3): 410–424.

Olavarria J and van Sluyters RC (1985) Organization and postnatal development of callosal connections in the visual cortex of the rat. *Journal of Comparative Neurology* 239(1): 1–26.

O’Leary DDM, Stanfield BB and Cowan WM (1981) Evidence that the early postnatal restriction of the cells of origin of the callosal projection is due to the elimination of axonal collaterals rather than to the death of neurons. *Developmental Brain Research* 227(4): 607–617.

Paul LK, Brown WS, Adolphs R, et al. (2007) Agenesis of the corpus callosum: Genetic, developmental and functional aspects of connectivity. *Nature Reviews Neuroscience* 8(4): 287–299.

Paxinos G, Halliday G, Watson C, et al. (2007) *Atlas of the Developing Mouse Brain: At E17.5, P0, and P6*. London: Elsevier.

Sohur US, Padmanabhan HK, Kotchetkov IS, et al. (2014) Anatomic and molecular development of corticostriatal projection neurons in mice. *Cerebral Cortex* 24(2): 293–303.

Suárez R, Fenlon LR, Marek R, et al. (2014) Balanced interhemispheric cortical activity is required for correct targeting of the corpus callosum. *Neuron* 82(6): 1289–1298.

Veinante P and Deschênes M (2003) Single-cell study of motor cortex projections to the barrel field in rats. *Journal of Comparative Neurology* 464(1): 98–103.

Wang C-L, Zhang L, Zhou Y, et al. (2007) Activity-dependent development of callosal projections in the somatosensory cortex. *Journal of Neuroscience* 27(42): 11334–11342.

Wilson CJ (1987) Morphology and synaptic connections of crossed corticostriatal neurons in the rat. *Journal of Comparative Neurology* 263(4): 567–580.

Yorke CH and Caviness VS (1975) Interhemispheric neocortical connections of the corpus callosum in the normal mouse: A study based on anterograde and retrograde methods. *Journal of Comparative Neurology* 164(2): 233–245.

Zhou J, Wen Y, She L, et al. (2013) Axon position within the corpus callosum determines contralateral cortical projection. *Proceedings of the National Academy of Sciences of the United States of America* 110(29): E2714–E2723.